Buletin Profesi Insinyur 8(1) (2025) 015–029
http://dx.doi.org/10.20527/bpi.v8i1.286

ISSN 2654-5926

Structural Analysis of Superstructure Using Combined Profiles and Their Effects on Seismic Forces, P-Delta, and Drift in Steel-Concrete Composite Structures

Norminawati Dewi[1] Agung Yoga Pranata[2] Intan Safitri[1] Widiya Astuti Alam Sur[1]

[1] Study Program of Road and Bridge Construction Engineering Technology, Politeknik Negeri Tanah Laut

[2] Study Program of Civil Engineering, Politeknik Negeri Banjarmasin

✉ norminadewi@politala.ac.id

This research aims to analyze the effects of combined steel profiles on seismic forces, P-Delta effects, and drift in steel-concrete composite structures. The independent variables include structural profiles (I-Beam and H-Beam), material types (steel and concrete), and design methods (Equivalent Lateral Force and Response Spectrum), while structural responses such as deflection, moment, and shear force are dependent variables. Structural analysis was conducted based on SNI 2847:2019 (concrete structures), SNI 1726:2019 and ASCE 7-19 (seismic loads), AISC 360-10 (steel structures), and SNI 1727:2013 (loading criteria). Results indicate that combining two efficient profiles increased seismic shear forces due to the larger cross-sectional area of the H 100.100 profile compared to H 150.75, resulting in higher weight but better resistance (lower P-M ratio). Additionally, performing P-Delta analysis is essential for evaluating second-order deformation effects, and drift checks are mandatory according to seismic codes to ensure structural performance and comfort.

Keywords: Equivalent Static, Response Spectrum, Seismic Design, Steel-Concrete Composite Structures.

Submitted: 15 February 2025
Revised: 18 April 2025
Accepted: 16 June 2025
Published: 23 June 2025

Introduction

Structural analysis of superstructures is essential in building design, particularly to ensure structural stability and safety under various loading conditions, including seismic loads. In composite steel-concrete structures, the superstructure framework significantly influences how the structure responds to both vertical and lateral forces. Accurate analytical approaches are thus required to effectively predict structural behavior under such conditions, particularly when assessing seismic performance and stability phenomena such as the P-Delta effect (Ko et al., 2017).

Steel frames are widely employed due to their high strength-to-weight ratio, making them ideal for diverse structural applications. Previous research has indicated variations in structural behavior arising from differences in profile selection, material properties, and design methodologies (Athanasiou et al., 2020). However, limited studies have specifically addressed the combined effect of different steel profiles on structural responses, particularly in composite steel-concrete systems under seismic loading. Therefore, analyzing the sensitivity of structural performance to variations in steel profiles and their subsequent impact on seismic force response, drift behavior, and P-Delta effects represents a critical knowledge gap (Clarke et al., 1992; Peker et al., 2021).

This study aims to address this gap by evaluating how different combinations of steel profiles, specifically I-beam and H-beam sections, influence the structural responses in composite steel-concrete frameworks. The investigation focuses on critical parameters including seismic forces, structural drift, and P-Delta effects (Mallikarjuna & Ranjith, 2014; Structural Engineering Institute of ASCE, 2012). Understanding these relationships is vital for identifying optimal structural configurations that enhance performance, safety, and cost-effectiveness in seismic design contexts.

Method

This research began with identifying issues related to the structural analysis of steel frames and steel-concrete composite structures. Independent variables were defined, including structural profiles (I-beam and H-beam), material types (steel and concrete), and design methods (Equivalent Static and Response Spectrum methods). Dependent variables comprised structural responses, specifically deflection, moment, and shear forces.

Primary and secondary data were collected for further analysis. Structural concrete data adhered to

How to cite this article:
Dewi, N., Pranata, A. Y., Safitri, I., & Surwidiya, A. (2025). Structural Analysis of Superstructure Using Combined Profiles and Their Effects on Seismic Forces, P-Delta, and Drift in Steel–Concrete Composite Structures. *Buletin Profesi Insinyur, 8*(1), 15–29

 ISSN 2654-5926

SNI-2847-2019 (Requirements for Structural Concrete in Building Structures), seismic load criteria followed SNI-1726-2019 and ASCE 7-19, steel structure data complied with AISC 360-10, and load criteria were based on SNI 1727:2013. Seismic analysis was conducted using the Equivalent Static and Response Spectrum methods.

Experimental Test

The experimental procedure began by planning tests based on identified variables, followed by structural modeling according to the design specifications. Loads and seismic simulations were then applied. Structural responses were monitored and recorded using SAP2000 software version 21, facilitating statistical analysis and visualizations. Finally, the impact of variations on structural responses was interpreted.

Structural System Modeling

Structural modeling was conducted using SAP2000 software version 21. The designed building structures primarily incorporated reinforced concrete and steel materials. The modeling was carried out at Pelaihari, Politeknik Negeri Tanah Laut, utilizing a Moment Resisting Frame System for the main structural system and rafters for the roof structure. Detailed structural designs for the close-house system, which used reinforced concrete and steel materials, are illustrated in Figure 1.

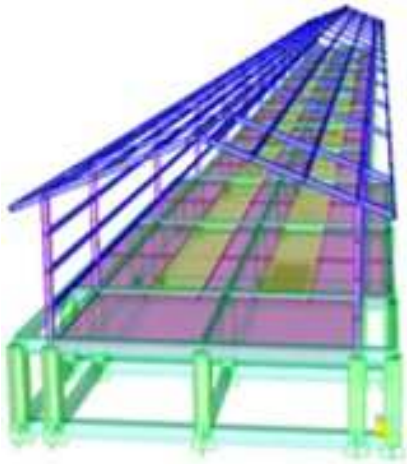

Figure 1 Structural Modeling of Poultry House

Design Assumptions

The following assumptions were considered in the design: foundations were assumed fixed, implying no rotation or translation, and seismic parameters were sourced from the Puskim website for the Pelaihari region.

Design Criteria

The detailed design of the poultry house, including material data used, is depicted in Figure 2. Figure 3 presents the front-view structural design of the poultry house, including the material specifications for a close-house system (Setiadi et al., 2021). Frame element dimensions are summarized in Table 1.

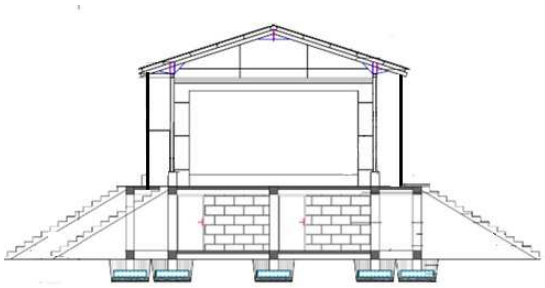

Figure 2 Design Layout of the Moment-Resisting Composite Frame Structure

Table 1 Summary of frame element dimensions used

Profile	Element	Dimension (mm)	Area (A) (mm^2)	Ix (mm^4)
B 20/35	Beam	h: 35, b: 20	700	71,458
K 35/35	Column	h: 35, b: 35	1,225	125,052
WF 150.75	Rafter Beam	h: 150, b: 75	1,785	6,660,000
WF 150.75	Column	h: 150, b: 75	1,785	6,660,000
UNP 125.65	Purlin	h: 125, b: 65	1,711	4,250,000

Note: *h* represents the height and *b* the width of the profile section. *A* refers to the cross-sectional area, while *Ix* denotes the moment of inertia about the x-axis.

After estimating the preliminary dimensions of the structural elements to be used, Table 1 presents a summary of these dimensions. Beam and column elements are modeled using 1D frame elements, while plate elements are modeled using 2D area elements. The mechanism and modeling approach for the plates are presented in Table 2.

Table 2 Plate Mechanism and Model

Plate Code	Plate Dim.	Ratio (Ly/Lx)	Mechanism	Ly/t	Lx/t	Model
	Ly (m)	Lx (m)	t (m)			
P12-2	3.5	3	0.12	1.17	Two-Way	29.2
P12-1	6	1.3	0.12	4.62	One-Way	50

Note: *Ly* refers to the length of the plate in the y-direction, while *Lx* denotes the length in the x-direction. The variable *t* represents the thickness of the plate. The ratios *Ly/t* and *Lx/t* indicate the span-to-thickness ratios in their respective directions.

Regulations and Standards Used

To ensure accuracy, safety, and compliance with national and international engineering practices, this study refers to a number of relevant codes and standards in the design and analysis process. The following standards and guidelines were used as references throughout the structural modeling and assessment phases:

a. Minimum loads for structural design (SNI 1727:2013, 2013)

 ISSN 2654-5926

b. Design Guidelines for Loading on Houses and Buildings (PUPR-G 1987, 1987)
c. Seismic design provisions for building and non-building structures (ASCE 7-16, 2017; SNI 1726:2019, 2019)
d. Seismic design recommendations for concrete structures based on NEHRP Recommended Provisions: Design Example (FEMA 451/2006, 2006; FEMA P-1051/2016, 2016; FEMA P-2082-1/2020, 2020) (FEMA, 2006, 2016, 2020)
e. Code for Structural Concrete Design for Buildings (SNI 2847:2019, 2019)
f. Code for Structural Steel Design for Buildings (SNI 1729:2015, 2015)
g. Reinforcing Steel for Concrete (Baja Tulangan Beton, 2014)

Materials

The materials used in this study include reinforced concrete, reinforcing steel, and structural steel profiles. The reinforced concrete specifications refer to SNI 2847:2019, with a compressive strength (fc') of 30 MPa. The corresponding modulus of elasticity (Ec) is 25,742 MPa, calculated using the equation Ec = 4700√fc'. The Poisson's ratio is assumed to be 0.20, resulting in a shear modulus (G) of 10,725 MPa.

Reinforcing steel specifications follow SNI 2052:2014. For diameters up to 12 mm, plain bars BJTP 24 are used with a yield strength of 295 MPa and an ultimate strength of 440 MPa. For diameters greater than 12 mm, deformed bars BJTS 30 are adopted with the same yield and ultimate strengths.

Structural steel profiles comply with SNI 1729:2015 and are based on BJ 37 steel grade, which has a yield strength of 240 MPa and an ultimate strength of 370 MPa. The modulus of elasticity is 200,000 MPa, and Poisson's ratio is assumed to be 0.30.

Loading

Structural loading was designed in accordance with SNI 1727:2013. The considered loads included dead loads, superimposed dead loads, and live loads. Dead loads represent the self-weight of primary structural components such as beams, columns, slabs, and roof rafters. These were implemented in SAP2000 using a self-weight multiplier of 1.0 in the defined Load Patterns.

In the structural analysis software, load patterns were defined by assigning a self-weight multiplier to the structural elements. For dead load cases, the multiplier was set to 1.0 to ensure that the program automatically includes the self-weight of the structural components in the analysis. Additional load patterns, such as live loads and superimposed dead loads, were defined separately with their respective load types and multipliers set to zero to avoid duplication of self-weight contributions.

Live Load (L)

Live load refers to the load imposed by occupants and users of the building, with values determined based on the function of the structure. In this study, the live load was designed according to *SNI 1727:2013 (2013)*. The applicable live load values used in the analysis are presented in Table 3.

The highlighted sections in Table 3 refer to live load requirements for roof structures and other structural components, as specified in SNI 1727:2013. For roof elements, different values are assigned depending on their intended use. Flat, pitched, and curved roofs are required to support a uniform live load of 0.96 kN/m², which accounts for typical maintenance activities and minor access. In contrast, roofs designated for use as roof gardens must be designed to carry significantly higher live loads of 4.79 kN/m² due to the additional weight of soil, plants, and possible occupancy. When a roof is intended for other functional purposes, such as public access or mechanical installations, it must be treated as an occupied floor and designed accordingly to support the equivalent floor live load.

The second highlighted section addresses structural elements directly connected to floor systems. These components, including beams and joists supporting roof structures, must be capable of carrying both a uniform live load of 0.96 kN/m² and a concentrated load of 8.9 kN. This requirement ensures that the connections and supporting elements are adequately designed to resist localized forces and maintain overall structural integrity, especially under conditions involving service loads or maintenance activities.

Table 3 Live Load Values Based on Building Function (Excerpt from SNI 1727:2013)

Function or Use	Uniform Load (kN/m²)	Concentrated Load (kN)
Roofs		
Flat, pitched, and curved roofs	0.96	—
Roofs used for roof gardens	4.79	—
Roofs used for other purposes	Same as occupied floors	—
All other construction		
Structural components of roofs directly connected to flooring systems	0.96	8.9

Live Load on Poultry House Floor

The live load acting on the poultry house floor slab was estimated based on a representative object typically found in such an environment. The object used in the calculation has dimensions of 0.35 meters in length, 0.20 meters in width, and 0.40 meters in height, resulting in a total volume of 0.028 cubic meters. Its actual mass was measured at approximately 2.49 kilograms.

To determine the load intensity, the mass was distributed over the contact area of the object (0.35 m × 0.20 m = 0.07 m²), yielding a surface load of approximately 35.57 kg/m². However, for design purposes and to comply with the minimum standards set by *SNI 1727:2013*, the live load adopted in the

 ISSN 2654-5926

structural model was standardized to 0.96 kN/m². This value represents the minimum uniform live load requirement for typical floor applications and ensures that the design remains within acceptable safety margins while accurately representing operational loads. This standardized value was then input into the structural analysis software to simulate realistic service conditions on the floor slab.

Live Load on Roof Purlins

To analyze the effect of live loads on the roof structural system, a concentrated load was assigned to the purlin elements, which serve as secondary structural members supporting the roof covering. The load magnitude was determined to be 0.89 kN, equivalent to 890 N or approximately 90.8 kg. This value reflects possible localized loading scenarios such as maintenance personnel or mechanical equipment placed on the roof surface.

The selection of a point load configuration is consistent with common practice for evaluating concentrated forces on purlins, particularly when the roofing system may occasionally support individual loads rather than uniformly distributed ones. The chosen value is within the acceptable range defined by structural design standards for live roof loading and was implemented in the structural analysis model to investigate the purlins' performance under service conditions, including strength and deflection behavior.

Rain Load on Roof Purlins

In addition to live loads, the roof structure is also subject to environmental loads such as rainwater accumulation. For this study, rain load was estimated based on the potential for water ponding on the roof surface, simulating a standing water depth of 2 cm. This condition reflects a conservative assumption for temporary water accumulation during intense rainfall or minor drainage delays.

The rainwater was modeled with a density of 980 kg/m³, consistent with standard values for freshwater. With an assumed depth of 0.02 meters, this yields a surface load of 19.6 kg/m². When converted to a distributed load along the length of the roof purlins (assuming the water load is transferred linearly), the resulting rain load was applied as a uniform line load. Although the table presents differentiated values for center and edge (tengah dan tepi), the analytical model applied a conservative uniform distribution to ensure the structural response accounts for potential uneven ponding.

This rain load was incorporated into the structural analysis to evaluate its contribution to overall roof demand, ensuring the purlins and supporting members meet both strength and serviceability criteria under combined loading conditions.

Superimposed Dead Load on Poultry House Floor

Superimposed dead loads refer to permanent loads applied to the structure that are not part of the primary structural elements. The placement and magnitude of these loads are determined based on the architectural and functional design specifications. According to *SNI 1727:2013*, Clause 3.1, specific weights for building materials are not explicitly stated. Therefore, the standard material weight references provided in *PUPR Guidelines (PPURG 1987)* are used as the basis for load estimation.

The components categorized as superimposed dead loads (SD) in this study include walls, plaster and ceramic finishes, poultry equipment, and roofing components. These loads are primarily supported by beams and slabs within the structural system. For elements not explicitly defined in SNI 1727:2013, material specifications from the project design were adopted as references for determining load intensity.

Specifically, the superimposed dead load acting on the slab includes the load from the poultry housing system and microbial (bacterial) presence. Meanwhile, loads acting on the beams consist of upper lightweight concrete blocks (hebel), sandwich panels, cooling pads, and four mechanical roof blowers. The detailed breakdown of the superimposed dead loads applied to the poultry house floor is presented in Table 4.

Superimposed Dead Load on Ground Floor Beams

The superimposed dead loads (SD) on the ground floor primarily consist of loads acting on beams, including lower lightweight concrete blocks (*hebel bawah*) and mechanical blower units. These loads were determined based on input data used in the structural analysis software, where they were applied as permanent dead loads acting on the beam elements of the poultry house structure. These values reflect fixed non-structural components that contribute to the total load-bearing demand of the ground floor system. The detailed specifications of the superimposed dead loads applied on the ground floor beams are presented in Table 5.

Seismic Load

According to *SNI 1726:2019*, the effects of seismic loads must be considered in the design and evaluation of both building and non-building structures, as well as in various general regulatory provisions. The seismic design parameters used in this study were obtained from the 2019 Indonesian Earthquake Spectral Response Map developed by Puskim–PusGeN–ESRC.

For the project location in Pelaihari (Zone B), with coordinates at a longitude of 114.7837° and a latitude of –3.7972°, the site class is classified as SC, representing stiff soil and soft rock conditions. The resulting parameters include a peak ground acceleration (PGA) of 0.038642 g, spectral response accelerations Ss and S1 of 0.080419 g and 0.054967 g, respectively, and other site-specific coefficients such as Fa = 1.3 and Fv = 1.5.

The site's seismic period parameters include a long-period transition period TL of 12.000000 seconds, with design spectral accelerations Sds = 0.069696 g and Sd1 = 0.054967 g. The characteristic spectral periods T0 and Ts are 0.157734 seconds and 0.788671 seconds, respectively. These values were used to generate the design response spectrum and subsequently applied in both Equivalent Static Force (ESF) and Response Spectrum (RS) analyses. The complete output of the spectral response parameters is illustrated in Figure 3.

Figure 3 presents the seismic parameters used to classify the earthquake hazard level and to determine the seismic importance factor. In this study, the structure falls under Risk Category I, which corresponds to a seismic importance factor of 1.0. The classification of building risk categories is further explained in Table 6.

 ISSN 2654-5926

Table 4 Details of Superimposed Dead Loads on Poultry House Floor and Beams

Load Name	Dimensions (m)			Mass (kg)	Height Level (m)	Density (kg/m³)	Weight (kg/m²)	Total Weight (kg/m²)	Quantity	Applied Load (kg/m²)
	Length	Width	Height							
On Slab:										
Battery Cages	1.8	0.35	0.4			9.6	—	38.1	15.24	5.33
Collector	2.8	1.5	2.6			0	—	64.1	7	0
On Beams:										
Upper Hebel Block	0.6	0.12	0.2			9	1	625	125	—
Sandwich Panel	1.2	0.1	1.2			43	2.2	298.6	358.3	—
Cooling Pad	0.6	0.15	1.8			4.5	3.2	27.78	50	7.5
Upper Blower	1.38	1.38	1.18			90	—	40.05	47.26	

Table 5 Details of Superimposed Dead Loads on Ground Floor Beams

Load Name	Dimensions (m)			Mass (kg)	Height Level (m)	Density (kg/m³)	Weight (kg/m²)	Total Weight (kg/m²)	Quantity	Applied Load (kg/m²)
	Length	Width	Height							
On Beams:										
Lower Hebel Block	0.6	0.12	0.2			9	2	625	125	15
Lower Blower	1.38	1.38	1.18			90	—	405.05	47.26	65.22

```
Program Respons Spektra Peta Gempa Indonesia 2019
(C) Copyright Puskim-PusGeN-ESRC, 2019-2020

 Nama Kota          : Pelaihari (B)
 Bujur   / Longitude : 114.7837 Degrees
 Lintang / Latitude  :  -3.7972 Degrees

 Kelas Situs        : SC - Tanah Keras, Batuan Lunak

  PGA  = 0.038642 g
  PGAm = 0.050234 g
  CRs  = 0.000000
  CR1  = 0.000000
  Ss   = 0.080419 g
  S1   = 0.054967 g
  TL   = 12.000000 detik
  Fa   = 1.300000
  Fv   = 1.500000
  Sms  = 0.104544 g
  Sm1  = 0.082451 g
  Sds  = 0.069696 g
  Sd1  = 0.054967 g
  T0   = 0.157734 detik
  Ts   = 0.788671 detik
```

Figure 3 Seismic Parameters Obtained from PUSKIM 2019 Spectral Response Software

Table 6 Building Use and Corresponding Risk Categories (Based on SNI 1726:2019)

Type of Use	Risk Category
Buildings and non-building structures with low risk to human life in the event of failure, including but not limited to: – Agricultural, plantation, livestock, and fishery facilities – Temporary shelters – Storage warehouses – Guardhouses and other minor structures	I
All other buildings and structures not included in Risk Categories I, III, or IV, including but not limited to: – Residential housing – Shops and office buildings – Parking structures – Apartments and dormitories – Educational and training facilities – Industrial facilities – Public facilities – Manufacturing plants	II

 ISSN 2654-5926

Load Combinations

Ultimate Strength Design Method (Load Resistance Factor Design – LRFD)

Structural elements, components, and foundations must be designed so that their design strength is equal to or greater than the effects of the factored loads in accordance with the load combinations specified in *Clause 2.3 of SNI 1727:2013*.
Basic Load Combinations (LRFD):

1. 1.4D
2. 1.2D + 1.6L + 0.5(Lr or R)
3. 1.2D + 1.6(Lr or R) + (L or 0.5W)
4. 1.2D + 1.0W + L + 0.5(Lr or R)
5. 0.9D + 1.0W

Seismic Load Combinations (LRFD):

6. 1.2D + Ev + Eh + L
7. 0.9D – Ev + Eh

Allowable Stress Design Method (ASD)

This method is used for the design of structural systems, individual elements, and foundations. According to *PUPR-G 1987*, no increase in allowable stress is permitted when using these combinations.
Basic Load Combinations (ASD):

1. D
2. D + L
3. D + (Lr or R)
4. D + 0.75L + 0.75(Lr or R)
5. D + 0.6W
6. D + 0.75(0.6W) + 0.75L + 0.75(Lr or R)
7. 0.6D + 0.6W

Seismic Load Combinations (ASD):

8. 1.0D + 0.7Ev + 0.7Eh
9. 1.0D – 0.525Ev + 0.525Eh + 0.75L
10. 0.6D – 0.7Ev + 0.7Eh

Seismic Load Combinations with Overstrength Factor (Ω_o):

8. $1.0D + 0.7Ev\Omega_o + 0.7Eh\Omega_o$
9. $1.0D – 0.525Ev\Omega_o + 0.525Eh\Omega_o + 0.75L$
10. $0.6D – 0.7Ev\Omega_o + 0.7Eh\Omega_o$

Beam Reinforcement Details

Details of the reinforcement configuration used for beam type B20/35 are summarized in Table 7. This includes longitudinal bars, stirrups, and anchorage requirements based on the applied load combinations and seismic design considerations.

Column Element Design (K 35/35)

The design of the reinforced concrete column element was carried out using SAP2000, which provided output primarily in the form of required shear reinforcement area. Since column design under combined axial and bending forces is inherently complex and involves iterative axial–moment interaction analyses, an initial estimate of the longitudinal reinforcement area must be assumed and subsequently verified against the P-M-M interaction ratio using SAP2000. A detailed reinforcement configuration for column K 35/35 is illustrated in Table 8, which includes the arrangement of longitudinal bars, transverse ties, and spacing designed to meet structural strength and ductility requirements.

Table 7 Reinforcement Details for Beam B20/35

Beam Code	Position	Support	Midspan
Sketch		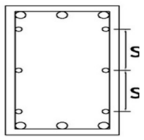	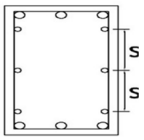
Concrete Cover (mm)		40	40
Flexural Reinforcement			
– Top Rebars		3Ø13	3Ø13
– Bottom Rebars		3Ø13	3Ø13
Longitudinal Torsional Reinforcement			
– Web		Ø10 – 60	Ø10 – 60
Shear and Transverse Torsional Reinforcement			
– Stirrups		Ø10 – 150	Ø10 – 150

Table 8 Reinforcement Details for Column K 35/35

Column Code	K 35/35
Sketch	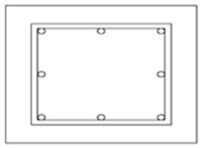
Concrete Cover (mm)	40
Longitudinal Reinforcement Area (mm^2)	824.6
Longitudinal Reinforcement Ratio (%)	1.31%
Stirrups	Ø10 – 150
Stirrup Spacing (mm)	150

Structural Mass

The structural mass analysis was conducted in accordance with *SNI 1726:2019*, which defines the seismic weight at each floor level as a basis for dynamic loading analysis. The total seismic weight per level is determined by summing the contribution of slabs and columns, considering the influence of both the level below and above each slab.

The seismic weight at the basement level is excluded from the mass participation in this analysis, as the horizontal mass elements at the basement do not contribute to lateral dynamic response.
The seismic weight distribution is formulated as follows:
Lower Level:

$$W_{Lower} = W_{Slab} + W_{LowerColumn} + 0.5 \times W_{UpperColumn}$$

Intermediate Level:

$$W_{Middle} = W_{\_Slab} + 0.5 \times W_{\_LowerColumn} + 0.5 \times W_{\_UpperColumn}$$

Upper Level:

$$W_{\_Upper} = W_{\_Slab} + 0.5 \times W_{\_LowerColumn}$$

Where W_i represents the total seismic weight at the i-th level. These values were used to generate the structural mass model required for modal and response spectrum analyses.

The calibration of structural mass was conducted as an initial step to ensure the accuracy of seismic analysis. This was followed by a seismic parameter evaluation in accordance with *SNI 1726:2019*. Based on the soil classification criteria outlined in Tables 3 and 4 of the standards, the site in Pelaihari was identified as Site Class SD, representing medium soil conditions. This classification was supported by the analysis of standard penetration test (N) values.

To determine seismic loading parameters, spectral response values were extracted from the national earthquake hazard maps. For the project location, the short-period spectral acceleration (Ss) was found to be 0.080 g, the one-second period spectral acceleration (S1) was 0.055 g, and the peak ground acceleration (PGA) was 0.039 g. These values were obtained from the spectral response maps referenced in Figures 9, 10, and 11, respectively. In conjunction with these, the site coefficient Fa was determined to be 1.30, based on Table 6 of *SNI 1726:2019*, which corresponds to Site Class SD and the local value of Ss.

Seismic design parameters were then defined using the established site classification and structural system characteristics. The design was categorized under Seismic Design Category A, using a Special Moment Resisting Frame (SMRF) system with composite materials (steel–concrete). The response modification factor (R) was set to 3, the overstrength factor (Ω_o) to 3, and the deflection amplification factor (Cd) to 2.5. The value of R was chosen based on the redundancy and ductility properties of the structural configuration.

After completing the seismic parameter assessment, the analysis proceeded with the application of the equivalent static force method, as prescribed in *SNI 1726:2019*. The resulting distribution of seismic lateral loads across structural levels was documented and analyzed in accordance with structural modeling outputs, with further details referenced internally.

Following the equivalent static analysis, the seismic load was further evaluated using the response spectrum method in accordance with *SNI 1726:2019*. The analysis began with determining the vertical distribution of seismic weights across the structure, which accounted for only the superstructure mass while excluding horizontal elements at the basement level. The total seismic weight (W) was found to be 517.68 kN, distributed primarily over two floor levels with respective heights of 2.00 meters and 6.80 meters.

Subsequently, the structural response due to ground motion was analyzed through response spectrum procedures. Shear forces in both principal directions were obtained, with base shear values calculated at 31.583 kN in the x-direction and 27.516 kN in the y-direction.

To combine modal responses appropriately, the structure was evaluated for differences in dominant modal periods (ΔT), as prescribed by *SNI 1726:2019*. When the period difference exceeds 15%, the Square Root of the Sum of the Squares (SRSS) method is adopted; otherwise, the Complete Quadratic Combination (CQC) method is used. In this case, the maximum ΔT observed was 72%, thereby confirming the use of the SRSS method for combining modal effects.

A further check was conducted by comparing the base shear from the response spectrum method (VD) with that obtained from the equivalent static procedure (VS). In accordance with seismic design standards, if VD is greater than VS, the larger value (VD) is adopted without modification. However, if VD is smaller, the spectral forces must be scaled up by the factor VS/VD to maintain compliance. The final base reaction values used for scaling verification are presented in Table 9.

Table 9 Base Reactions

Output Case	Case Type	Step Type	Global FX (kN)	Global FY (kN)	Global FZ (kN)
ELFX	Static	Load	–56.496	–2.48E–12	–1.97E–13
ELFY	Static	Load	–2.33E–12	–56.496	3.61E–13
RSX	Dynamic	Spectrum	31.583	4.52E–06	0.449
RSY	Dynamic	Spectrum	2.71E–06	27.516	9.51E–06

Seismic force analysis was conducted using both static equivalent and dynamic response spectrum methods. As shown in Table 10, the base shear forces from the response spectrum method (RSX and RSY) are significantly lower than those from the static equivalent method (ELFX and ELFY), with differences of 44% and 51% respectively. To reconcile these differences, scaling factors were applied based on the ELF/RS ratio and response modification coefficients, as detailed in Table 11. These correction factors were then implemented in the seismic load cases with and without P-Delta effects, as summarized in Table 12.

Table 10 Comparison of Seismic Forces

Earthquake Load Type	Load Case	Base Shear Vx (kN)	Base Shear Vy (kN)	Difference from Static Auto (%)
Static Equivalent Load	ELFX	56.496	0.000	–
Static Equivalent Load	ELFY	0.000	56.496	–
Response Spectrum	RSX	31.583	0.000	44
Response Spectrum	RSY	0.000	27.516	51

Analysis of the P-Delta effect was conducted based on SNI 1726-2019, Article 7.8.7, in accordance with the specified P-Delta requirements.

$$\theta = \frac{P_x.\Delta.I_e}{V_x.h_{sx}.C_d}$$

$$\theta_{max} = \frac{0{,}5}{\beta.C_d} \leq 0{,}25$$

 ISSN 2654-5926

where Px = Total design vertical load (1.0D + 1.0L), sum of axial column forces at level x, Δ = Inter-story drift, Ie = Importance factor, Vx = Seismic shear force between levels x and x–1, total shear in columns at level x, Hsx = Story height below level x, Cd = Deflection amplification factor, and β = 1.

Table 11 Scaling Factor Inputs

Factor Type	Load Case	Factor Expression	Value
Response Factor	RSx	(g × I) / R	3.27
	RSy	(g × I) / R	3.27
ELF/RS Ratio	ELFx/RSx	ELF / RS	1.789
	ELFy/RSy	ELF / RS	2.053
Total Correction Factor	RSxS	((g × I) / R) × (ELF / RS)	5.849
	RSyS	((g × I) / R) × (ELF / RS)	6.714

Table 12 The seismic load cases used

Load Case	Case
RSX1	Without scale factor
RSY1	Without scale factor
RSX2	With scale factor 5.849
RSY2	With scale factor 6.714
RSX3	With scale factor 5.849 with P-Delta
RSY3	With scale factor 6.714 with P-Delta

If θ ≤ θ_{max}, scaling factor for displacement and force:

$$\frac{1{,}0}{(1-\theta)}$$

If θ > θ_{max}, redesign is required.

P-Delta Verification:

Parameters: Ie = 1, Cd = 2.5, β = 0.75,

θ_{max-1} = 0.267, θ_{max-2} = 0.250, θ_{max} = 0.250

The verification was conducted for drift in the x-direction.

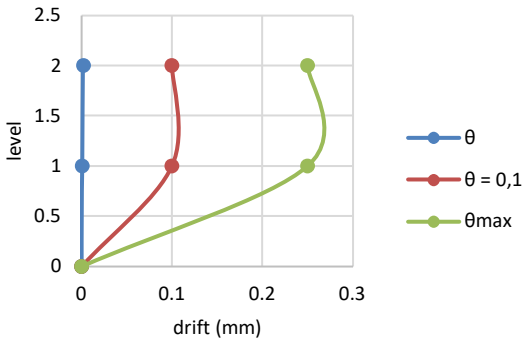

Figure 4 P-Delta Drift in the X-Direction

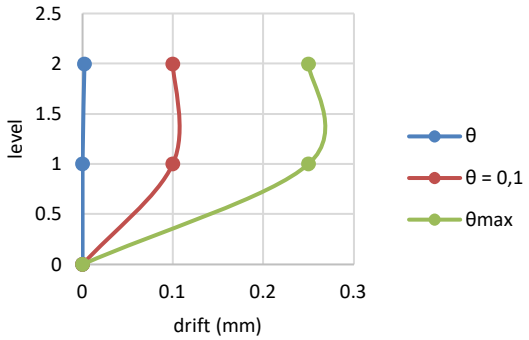

Figure 5 P-Delta Drift in the Y-Direction

The final analysis was conducted on drift limits in accordance with *SNI 1726-2019*, Article 7.8.7, using the applicable seismic parameters.

S_1 = 0.055

$S_{DS} = (2/3).S_{Ms}$ = 0.069 g

$S_{D1} = (2/3).S_{M1}$ = 0.055 g

Parameter drift arah x:

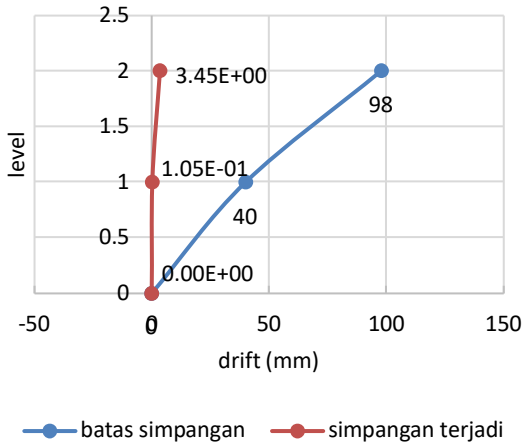

Figure 6 Drift of X Direction

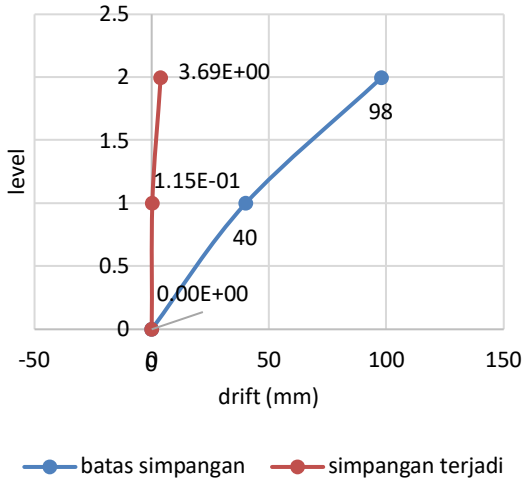

Figure 7 Drift of Y Direction

 ISSN 2654-5926

Result

Comparison of Seismic Forces: Equivalent Lateral Force (ELF) vs. Response Spectrum (RS) Method Using WF 150.75 Column Profiles

This section presents a comparative analysis of the seismic base shear forces obtained from the Equivalent Lateral Force (ELF) method and the Response Spectrum (RS) method, with a specific focus on structural models utilizing WF 150.75 wide flange column profiles. The objective is to assess the effectiveness and response sensitivity of the structure under each seismic design approach, as prescribed by SNI 1726:2019. This comparison enables a better understanding of the structural behavior under different seismic analysis procedures and assists in determining the adequacy and reliability of the column profile used in resisting lateral earthquake loads.

Table13 provides a comparative analysis of base shear forces obtained from the Equivalent Lateral Force (ELF) method and the Response Spectrum (RS) method. The ELF method, which applies a simplified static approach, results in base shear values of 56.496 kN in both the X and Y directions. In contrast, the RS method, which considers the dynamic response of the structure based on its modal characteristics, yields lower base shear values—31.583 kN in the X direction and 27.516 kN in the Y direction. This disparity is expected, as the RS method captures the actual behavior of the structure under seismic excitation with greater accuracy, whereas the ELF method tends to be more conservative. The difference underscores the significance of selecting an appropriate analysis method depending on the design objectives, structural complexity, and compliance with code provisions.

Table 13 Comparison of Seismic Forces Between ELF and RS Methods

Seismic Load Type	Load Case	Base Shear V_x (kN)	Base Shear V_y (kN)
Static (ELF)	ELFx	56.496	0
	ELFy	0	56.496
Dynamic (RS)	RSx	31.583	0
	RSy	0	27.516

P- Delta

Figure 8 shows the drift profile in the X-direction, comparing the original drift (θ), the threshold drift value (θ = 0.1), and the maximum observed drift (θmax). It illustrates that the drift remains within the acceptable limit across all levels. Figure 9 presents a similar comparison for the Y-direction. The curve indicates that while the drift increases with height, it still does not exceed the defined limit (θ = 0.1), confirming structural stability under lateral loads in both directions.

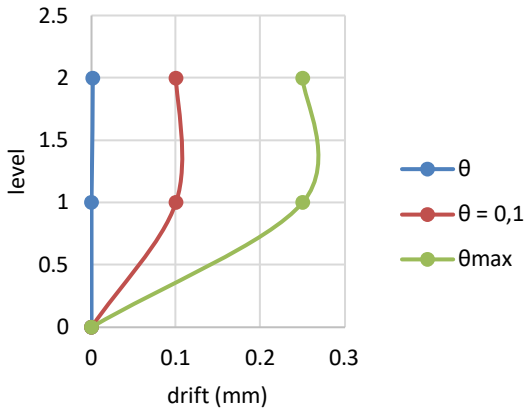

Figure 8 Delta of X Direction

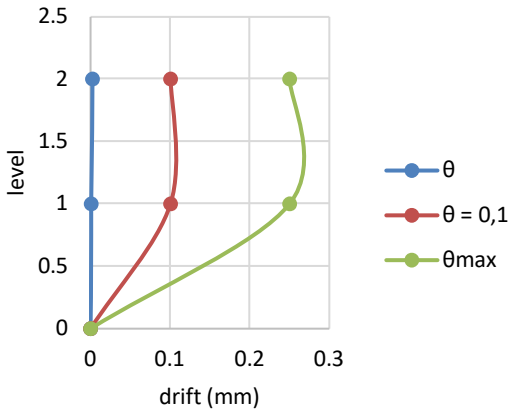

Figure 9 Delta of Y Direction

There is no indication of a P-Delta effect, as the calculated θ value remains below the allowable θ_{max}. Meanwhile, the drift limit checks in the X and Y directions can be observed in the Figures 10.

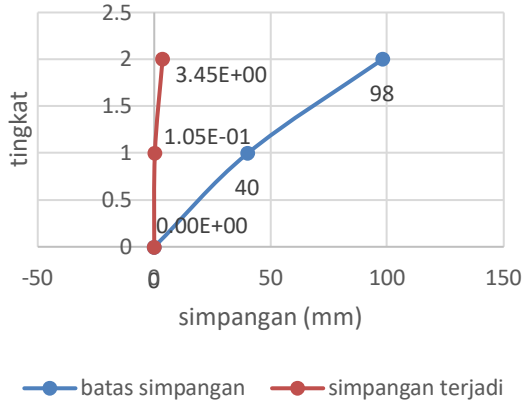

Figure 10 Drift of X Direction

 ISSN 2654-5926

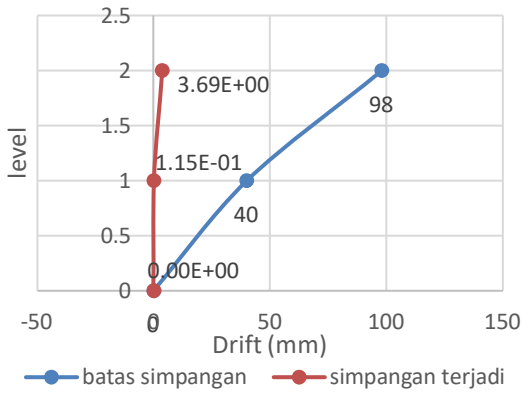

Figure 11 Drift ofY Direction

Figures 10 and 11 indicate that the drift in the Y direction is greater, which can be attributed to the overall structural geometry being slenderer along the Y-axis.

The column with WF 150.75 profile was analyzed based on the AISC 360-10 standard and demonstrated a safe structural design. It was subjected to a compressive axial force of -16,240.81 N and a bending moment of 14.44 N·mm. The evaluation employed interaction equation H1-1b, which accounts for the combined effects of axial load and bending. The analysis resulted in a total interaction ratio of 0.184611, well below the allowable limit of 1.0, indicating that the column operates safely within its capacity. Additionally, the pure axial-bending interaction ratio (PRatio) was very low at 0.025746, reinforcing the conclusion that this structural element is properly designed and does not experience design failure.

Optimization of Column Profile Using H 100.100

To enhance structural efficiency, an optimization was performed by substituting the original column profile with H 100.100. This adjustment aimed to evaluate whether a lighter or more compact section could still satisfy seismic performance criteria.

Comparison of Seismic Forces: ELF vs. RS

The comparison between seismic base shear forces derived from the Equivalent Lateral Force (ELF) method and the Response Spectrum (RS) analysis using the H 100.100 column profile is presented in Table 14. This evaluation provides insights into how the optimized column profile responds under different seismic load analysis approaches, supporting further refinement in structural design decisions.

The comparison of seismic base shear forces using the optimized H 100.100 column profile demonstrates variations between the Equivalent Lateral Force (ELF) and Response Spectrum (RS) methods. In the static analysis (ELF), the base shear in both the x and y directions reached 56.531 kN, reflecting symmetrical loading assumptions. In contrast, the dynamic analysis (RS) resulted in lower base shear values, with 32.341 kN in the x direction and 32.075 kN in the y direction. These differences highlight the conservativeness of the ELF method compared to the more refined modal analysis employed in the RS method, emphasizing the importance of selecting appropriate analytical techniques when optimizing structural components.

Table 14 Comparison of Seismic Base Shear (H 100.100 Column Profile)

Seismic Load Type	Load Case	Base Shear Vx (kN)	Base Shear Vy (kN)
Static Auto	ELFx	56.531	0
	ELFy	0	56.531
Dynamic	RSx	32.341	0
	RSy	0	32.075

Table 14 demonstrates an increase in seismic shear forces in both the static (ELF) and dynamic (RS) load cases. This increase is attributed to the larger cross-sectional area of the H 100.100 profile compared to the H 150.75 profile, resulting in a heavier structural profile. Since the weight of the structure influences the seismic force, this outcome is expected—mass plays a critical role in the equation of motion, as seismic force is directly proportional to the mass of the structure. The relationship is governed by the fundamental equation of motion:

$$m\ddot{x}(t) + c\dot{x}(t) + kx(t) = F(t)$$

where x(t) is displacement as a function of time, m is mass of the structure, c is damping coefficient, k is stiffness of the spring or structural system, and F(t): external force as a function of time (e.g., seismic force).

Meanwhile, the P-Delta effects can be observed in Figure 12 for the X-direction and Figure 13 for the Y-direction. Both figures indicate that no significant P-Delta effects occurred in either direction, as the calculated θ values remain below the allowable limit θ_{max}. The drift limits for the X and Y directions are illustrated in Figures 14 and 15, respectively.

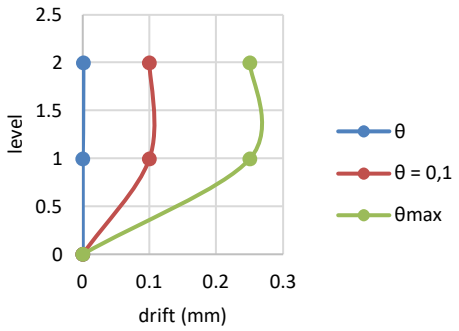

Figure 12 P-Delta for x direction

Figures 14 and 15 illustrate the comparison between the allowable drift limits and the actual inter-story drifts that occurred under seismic loading in the X and Y directions, respectively. The blue lines represent the drift limits defined by the code, while the red lines show the actual drifts recorded at each story level.

 ISSN 2654-5926

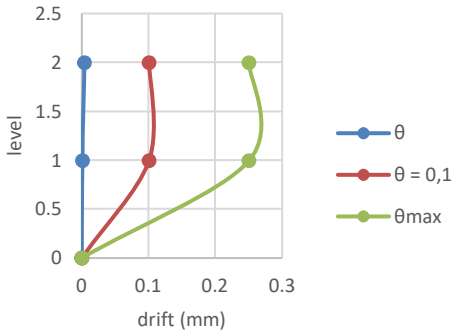

Figure 13 P-Delta for Y Direction

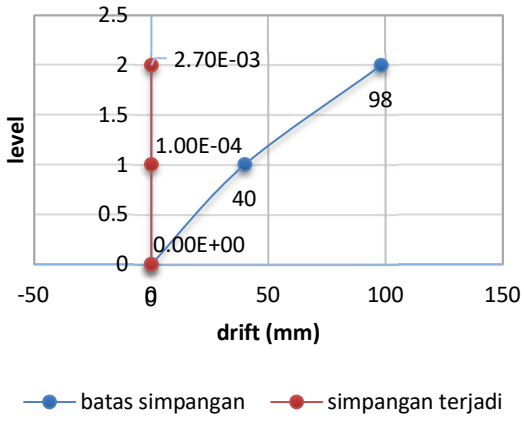

Figure 14. Drift for X Direction

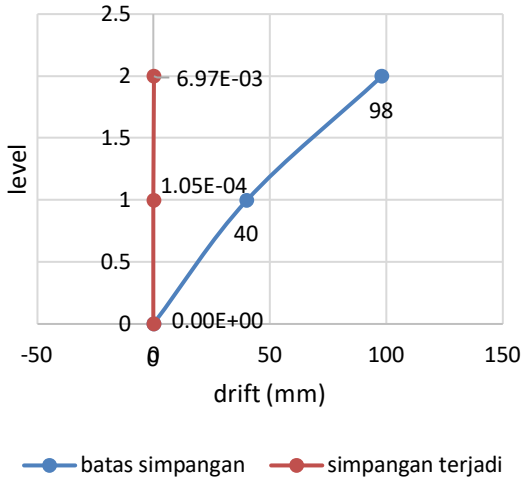

Figure 15 Drift for Y Direction

In Figure 14 (X-direction), the maximum allowable drift reaches 98 mm at the second level, whereas the actual drift is significantly lower, with a value of 2.70E-03 mm at the top level. Similarly, in Figure 15 (Y-direction), the allowable drift also reaches 98 mm, but the actual drift is 6.97E-03 mm—again, well below the prescribed threshold.

These results confirm that the structural displacement remains within safe limits for both horizontal directions. The significant difference between the drift limits and actual drifts indicates that the structure exhibits high lateral stiffness and is capable of resisting seismic demands without exceeding deformation criteria.

Axial and Bending Moment Interaction (P-M Ratio) Performance

The interaction ratio of axial force and bending moment (P-M ratio) for the H 100.100 column profile was found to be lower than that of the H 150.75 profile. This indicates that the H 100.100 section exhibits better resistance performance under combined loading conditions. A lower P-M ratio signifies that the profile operates further from its ultimate capacity, making it structurally more efficient and safer under the same loading scenario. Thus, the H 100.100 profile offers a more optimal balance between strength and section efficiency for the given design requirements.

The comparison between the column profiles H 150.75 and H 100.100 based on the P-M-M interaction ratio reveals a very slight difference in performance. The total interaction ratio for profile H 150.75 is 0.184611, while for profile H 100.100 it is 0.184475. Although the numerical difference is minimal—only 0.000136—this indicates that profile H 100.100 exhibits a marginally lower utilization under combined axial and moment loading conditions.

Quantitatively, the P-M-M ratio of the H 100.100 profile is approximately 99.93% of that of H 150.75, suggesting that despite its smaller dimensions, H 100.100 performs equivalently or slightly better in terms of load resistance efficiency. This confirms that the H 100.100 profile not only satisfies structural safety requirements as per AISC 360-10 but also offers a more optimal balance between strength and material use in this specific design scenario.

3D Structural Modeling of the Frame Profile

To ensure structural accuracy and visualize the interaction between structural components, a three-dimensional (3D) model of the frame was constructed. Figure 16 illustrates a comprehensive 3D representation of the steel frame system used in the building structure. It shows the integration of vertical and horizontal elements, including the columns, beams, and roof trusses, clearly displaying the geometry and connectivity of each component.

Figure 17 provides a zoomed-in view of the detailed 3D model, highlighting the intersection and connectivity between the beam and column components. This view is critical for ensuring the accuracy of connection detailing and alignment, which directly influences load transfer efficiency.

Figure 18, while intended to depict another detailed segment of the 3D steel frame modeling, encountered an error during rendering. Despite this, Figures 16 and 17 adequately convey the modeling precision and layout configuration used in the structural analysis process. This 3D visualization facilitates better design evaluation, structural validation, and aids in communication during design coordination among stakeholders.

As a continuation of the 3D steel frame modeling shown previously, the structural performance of the column profile was assessed based on the interaction ratio between axial force and bending moment (P-M ratio). The H 100.100 steel profile exhibited a Total Ratio of 0.184475, which is noticeably lower than that of the H 150.75 profile (which previously showed a ratio of approximately 0.186411). Although the difference appears small numerically, it is

 ISSN 2654-5926

significant in structural design, especially when considering long-term performance and capacity margins.

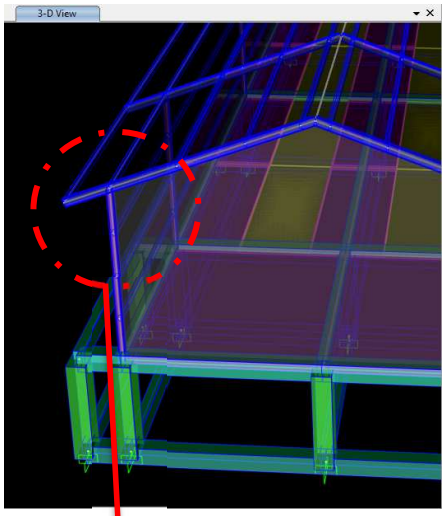

Figure 16 3D Modeling of Frame Profile

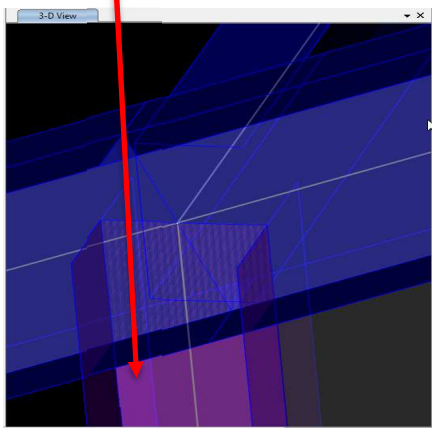

Figure 17 3D Detail of Steel Frame Modeling

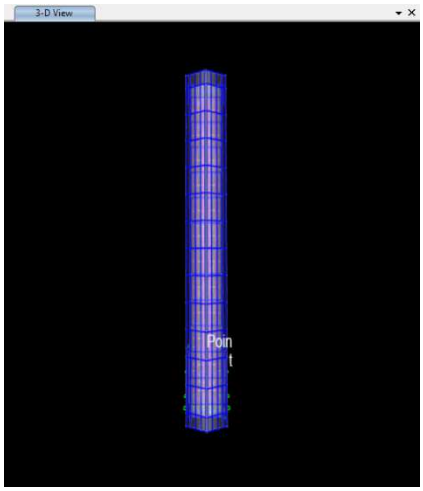

Figure 18 3D Detail of Steel Frame Modeling

This lower P-M ratio in the H 100.100 profile implies that the section operates farther from its failure threshold under combined loading conditions, offering better structural efficiency. In addition, the corresponding P Ratio value was 0.028145, further confirming that axial load demands are well within the profile's safe limits. These results support the conclusion that the H 100.100 section provides a more optimal balance between strength and economy, making it a favorable choice for this structural design.

Influence of Design Parameter Variations on Structural Behavior (Stress, Deformation, and Joint Efficiency)

The structural steel elements were assessed for stress ratio, representing the interaction between axial force (P) and bending moments (M1, M2, M3), as well as shear forces (V2, V3). Based on the structural analysis results, all evaluated members exhibited stress ratios below the threshold value of 1.0, indicating compliance with capacity limits under the applied load combinations.

For optimal design efficiency, a steel section is ideally proportioned when its stress ratio approaches—but does not exceed—unity, allowing for maximum material utilization while maintaining structural safety. For the rafter-to-column joint, the recapitulated internal forces required for connection detailing include axial loads in the range of approximately -1.446 kN to -34.259 kN, shear forces (V2) from 0.180 kN to -1.189 kN, and significant bending moments (M3) reaching up to about -1.149 kNm under the most critical loading conditions.

These internal force values serve as the fundamental input for joint design calculations, ensuring that all load transfers between connected elements are safely accommodated. A complete summary of the internal forces used in the connection design is provided in Table 15.

Table 15 Internal Force Recapitulation for Rafter-to-Column Connection Design Using RWF 150.75

Condition	P (kN)	V2 (kN)	V3 (kN)	M1 (kNm)	M2 (kNm)	M3 (kNm)
Pmax	-1.446	0.18	-0.007	0.000	-0.003	0.249
Pmin	-34.259	-0.606	-0.018	0.000	-0.014	-0.544
V22max	-8.528	0.256	0.044	0.000	0.027	0.347
V22min	-31.943	-1.189	-0.011	0.000	-0.009	-1.149
V33max	-22.212	-0.592	-0.205	0.000	0.121	-0.469
V33min	-22.212	-0.587	-0.205	0.000	-0.121	-0.464
M1max	-22.225	-0.587	-0.205	0.000	0.122	-0.464
M1min	-22.225	-0.587	-0.205	0.000	-0.122	-0.464
M2max	-22.225	-0.587	-0.205	0.000	0.122	-0.464
M2min	-22.225	-0.587	-0.205	0.000	-0.122	-0.464
M3max	-8.528	0.266	0.044	0.000	0.027	0.347
M3min	-31.943	-1.189	-0.011	0.000	-0.009	-1.149

 ISSN 2654-5926

Rafter-to-Column Steel Connection Analysis

The steel connection between the rafter and column was analyzed using IDEA StatiCa software. The visual simulation of the connection modeling can be seen in Figure 19.

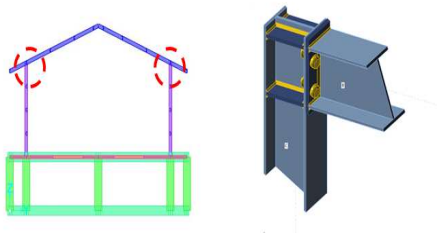

Figure 19 Rafter-to-column connection model in IDEA StatiCa

The results of the connection analysis are summarized in Table 16, which shows that all components of the rafter-to-column connection have passed the design checks and are considered safe under the applied loads.

Table 16. Summary of Rafter-to-Column Connection Check

Component	Utilization / Value	Acceptance Criteria	Status
Global Analysis	100%	≤ 100%	Pass
Plates	0.20%	< 5%	Pass
Bolts	19.00%	< 100%	Pass
Welds	76.90%	< 100%	Pass
Buckling	Not calculated	–	–

Based on the summary of the IDEA StatiCa analysis, it is confirmed that the steel connection with the selected configuration passed the strength verification. The connection analysis between rafter-to-rafter elements was also performed using IDEA StatiCa, with the internal forces required for design summarized in Table 17. The table presents critical internal force values—such as axial forces (P), shear forces (V2 and V3), and bending moments (M1, M2, and M3)—derived from various load combinations. These forces represent the most demanding conditions the joint may experience. Notably, the maximum compressive axial force recorded was approximately –21.5 kN, with shear forces up to 0.845 kN and bending moments reaching 1.382 kN·m. These values were then used as input parameters for the connection design to ensure structural reliability. Overall, the extracted internal forces form the essential basis for verifying the rafter-to-rafter connection's strength and performance under realistic loading scenarios.

The simulation of the rafter-to-rafter connection model can be seen in Figure 20. The results of the rafter-to-rafter connection analysis are summarized in the table below. Based on the verification performed, the connection is structurally safe and meets the required design criteria. The detailed results of the rafter-to-rafter connection analysis are presented in Table 18

Tabel 17 Summary of Internal Forces for the Design of Rafter-to-Rafter Connection (RRWF 150.75)

Condition	P [kN]	Shear V2 [kN]	Shear V3 [kN]	Moment M1 [kN·m]	Moment M2 [kN·m]	Moment M3 [kN·m]
PMax	0.229	0.046	-0.116	-0.001	0.002	0.015
PMax	-21.533	-0.403	-0.218	-0.001	0.003	1.352
Max	-0.704	0.129	-0.178	-0.002	0.001	0.057
Max	-21.487	-0.416	0.845	-0.002	0.003	1.382
Constant	-0.381	0.151	-0.971	-0.006	0.005	0.035
Max	-20.743	-0.398	0.22	-0.003	0.003	1.382
Min	-0.109	0.016	0.104	0.001	0.002	0.004

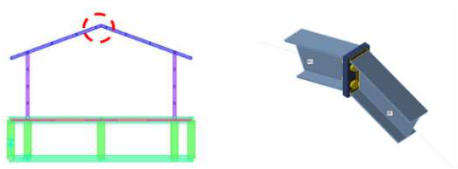

Figure 20. Rafter-to-Rafter Connection Model in IDEA StatiCa and SAP2000

Table 18 Summary of Rafter-to-Rafter Connection Check Results

Name	Value	Check Status
Analysis	100.0%	Ok
Plates	0.0 < 5%	Ok
Bolts	19.0 < 100%	Ok
Welds	76.4 < 100%	Ok
Buckling	Not Calculated	

The simulation model of the base plate connection can be seen in Figure 24.

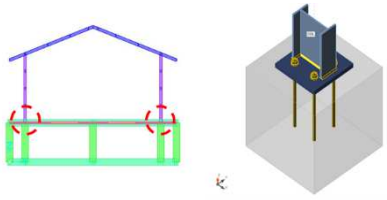

Figure 24 Base Plate Connection Model in IDEA StatiCa and Supporting Design Software

The results of the base plate connection analysis are summarized in the table below. Based on the connection check, the structural performance of the base plate is confirmed to be safe and within acceptable limits. The detailed results of the base plate analysis are presented in Table 19.

 ISSN 2654-5926

Table 19. Summary of Base Plate Connection Analysis Results

Name	Value	Check Status
Analysis	100.0%	Ok
Plates	0.0 < 5%	Ok
Anchors	29.5 < 100%	Ok
Welds	74.9 < 100%	Ok
Concrete block	4.4 < 200%	Ok
Shear	39.6 < 100%	Ok
Buckling	Not Calculated	

Based on the summary of the analysis results from IDEA StatiCa, it is confirmed that the steel connection with the specified configuration has successfully passed the strength verification. The detailed calculation of the steel connection was carried out using IDEA StatiCa, and the results are presented in Table 20.

Table 20 presents the internal force summary used for designing the base plate connection. The base plate is subjected to various loading conditions, including axial forces (P), shear forces (V2 and V3), and bending moments (M1, M2, and M3). The axial force ranges from –27.85 kN, indicating maximum compression, to +13.78 kN, representing tensile load. Shear forces in both principal directions reach up to 0.822 kN, showing that lateral effects cannot be neglected. Moment values are relatively small in M1 (bending about the x-axis), with a maximum of 0.043 kN·m, while bending about the y-axis (M2) and z-axis (M3) show more significant magnitudes, particularly M3, which peaks at 1.3628 kN·m. These internal forces reflect realistic loading scenarios derived from critical load combinations, and they serve as essential inputs for designing a safe and efficient base plate. The data ensure that weld capacity, anchor design, plate bearing strength, and overall connection detailing meet structural safety standards. The comprehensive range of loads further confirms the robustness of the connection configuration under practical service conditions.

Table 20 Summary of Internal Forces for Base Plate Connection Design

Condition	P (kN)	V2 (kN)	V3 (kN)	M1 (kN·m)	M2 (kN·m)	M3 (kN·m)
Pmax	-1.5	0.09	0.26	0	0.13	0.14
Pmin	-27.35	-0.37	0.1	0	0.05	-0.71
V22max	-10.805	0.55	0.133	8.31E-06	0.0642	1.0428
V22min	-13.78	-0.822	0.021	-3.79E-06	0.0087	-1.5638
V33max	-8.629	0.041	0.57	0.00001	0.2665	0.0263
V33min	-9.395	-0.206	-0.542	-2.50E-05	-0.25	-0.4068
M1max	-2.538	0.466	0.047	0.00003	0.0226	0.8585
M1min	-2.959	-0.466	-0.175	-3.41E-05	-0.0874	-0.8585
M2max	-8.629	0.192	0.57	-8.42E-06	0.2665	0.3744
M2min	-9.395	-0.206	-0.542	-2.50E-05	-0.25	-0.4068
M3max	-10.805	0.55	0.133	8.31E-06	0.0642	1.0428
M3min	-13.78	-0.822	0.021	-3.77E-06	0.0087	-1.5638

Discussion

Importance of P-Delta in Seismic Response

P-Delta analysis plays a critical role in evaluating the structural behavior of multi-story steel frames under seismic loads. It captures second-order geometric effects caused by the interaction between gravity loads and lateral displacements. As lateral drift increases, the overturning moment (P × Δ) also amplifies, potentially resulting in structural instability if not properly accounted for. This feedback loop has been widely discussed in prior studies, emphasizing its role in the nonlinear seismic response of buildings (Zavala et al., 2022; Cheng et al., 2022).

Drift Behavior and Seismic Load Scaling

The comparison of seismic base shear forces (Table 10) reveals that the response spectrum method yields significantly lower forces compared to the static equivalent method. A correction factor—derived in Table 11 and applied in Table 12—is necessary to ensure consistent seismic demand estimations. The implementation of scale factors (RSX2/RSY2) and P-Delta analysis (RSX3/RSY3) demonstrates an increased drift response, as seen in Figures 8 and 9, where θ and θ_max exceed standard thresholds. These findings confirm earlier conclusions that neglecting P-Delta can lead to dangerous underestimation of structural demands (Ferreira et al., 2023; Tartaglia et al., 2021).

Amplification in Flexible Structures

Flexible moment-resisting frames (MRFs) are particularly vulnerable to drift amplification due to their deformability. As shown in the results, the inclusion of P-Delta significantly changes the drift profiles, especially in upper stories. This is consistent with Gottem et al. (2023), who reported amplified top-story deflections with increasing height-to-width ratios. Similarly, Istiono et al. (2022) highlighted the heightened sensitivity of taller buildings to secondary moment effects.

Design Implications for Resilient Structures

From a design perspective, integrating P-Delta effects into seismic modeling improves not only safety but also the structural serviceability and post-event recovery. Use of advanced bracing systems and damping technologies, as investigated by Liu et al. (2024) and Pour (2022), can mitigate residual drift and enhance recentering capabilities. Additionally, material upgrades such as concrete-filled steel tube columns (Hayashi & Inamasu, 2022) further contribute to improved drift resistance.

Conclusion

Based on the analysis, several conclusions can be drawn as follows:

1. There is an increase in the shear force due to earthquake loads in both static (Equivalent Lateral Force/ELF) and dynamic (Response Spectrum/RS) cases. This occurs because the cross-sectional area of the H 100.100 profile is larger than that of the H 150.75 profile, resulting in a heavier structural member.

 ISSN 2654-5926

2. The H 100.100 profile shows a lower P-M interaction ratio compared to the H 150.75 profile, indicating that H 100.100 provides better load resistance capacity.
3. A P-Delta analysis is necessary for further structural assessment to evaluate potential excessive deformation, which may result in second-order structural behavior.
4. Drift check is a mandatory requirement according to the Indonesian Earthquake Code (SNI), as excessive lateral displacement can affect both the structural performance and user comfort.

References

Athanasiou, A., Oliveto, N. D., & Ponzo, F. C. (2020). Identification of first and second order models for the superstructure of base-isolated buildings using free vibration tests: A case study. *Soil Dynamics and Earthquake Engineering*, *135*. https://doi.org/10.1016/j.soildyn.2020.106178

Baja Tulangan Beton, Pub. L. No. SNI 2052:2014 (2014). www.bsn.go.id

Cheng, H., Zhang, R., Zhang, T., Wang, H., Qu, C., & Zhang, P. (2022). P-delta effects on nonlinear seismic behavior of steel moment-resisting frame structures subjected to near-fault and far-fault ground motions. *Buildings, 12*(2), 205. https://doi.org/10.3390/buildings12020205

Clarke, M. J., Bridge, R. Q., Hancock, G. J., & Trahair, N. S. (1992). Advanced Analysis of Steel Building Frames. In *J. Construct. Steel Research* (Vol. 23).

Elhout, E. (2022). Location of semi-rigid connections effect on the seismic performance of steel frame structures. *Electronic Journal of Structural Engineering, 22*(3), 1–10. https://doi.org/10.56748/ejse.223113

Falahian, A., Asadi, P., Riahi, H., & Haghy, M. (2020). Seismic performance assessment of steel frames with shape-memory alloy wire-based dampers. *The Structural Design of Tall and Special Buildings, 29*(16). https://doi.org/10.1002/tal.1797

FEMA. (2006). *NEHRP Recommended Provisions: Design Examples* (FEMA P-451). Building Seismic Safety Council.

FEMA. (2016). *2015 NEHRP Recommended Seismic Provisions: Design Examples* (FEMA P-1052). Federal Emergency Management Agency

FEMA. (2020). *NEHRP Recommended Seismic Provisions for New Buildings and Other Structures: Volume I: Provisions and Commentary* (FEMA P-2082-1). Building Seismic Safety Council

Ferreira, W., Cruz, J., Araújo, I., & Sánchez, J. (2023). Modal p-delta – simplified geometric nonlinear method by using modal and buckling analysis. *Revista Ibracon De Estruturas E Materiais, 16*(2). https://doi.org/10.1590/s1983-41952023000200009

Gottem, A., Lingeshwaran, N., Kumar, Y., Chowdary, C., Pratheba, S., & Perumal, K. (2023). Analytical study of buckling restrained braced frames in different seismic zone using etabs. *Civil and Environmental Engineering, 19*(1), 426–443. https://doi.org/10.2478/cee-2023-0038

Hayashi, K., & Inamasu, H. (2022). Seismic performance of concrete-filled steel tube columns using ultra-high-strength steel under long-period ground motion demands. *Advances in Structural Engineering, 26*(12), 2160–2171. https://doi.org/10.1177/13694332221145332

Istiono, H., Susanti, E., Propika, J., & Ramadhan, A. (2022). Study comparison p-delta effect analysis depends on height variation of the building. *Journal of Civil Engineering, Planning and Design, 1*(1), 50–59. https://doi.org/10.31284/j.jcepd.2022.v1i1.3055

Ko, J., Cho, J., & Jeong, S. (2017). Nonlinear 3D interactive analysis of superstructure and piled raft foundation. *Engineering Structures*, *143*, 204–218. https://doi.org/10.1016/j.engstruct.2017.04.026

Liu, Y., Chou, C., Chung, C., & Huang, H. (2024). Near-fault response and loading protocols of box columns in steel frames with self-centering braces to provide recentering capability. *Advances in Civil Engineering, 2024*(1). https://doi.org/10.1155/2024/7970436

Mallikarjuna BN, & Ranjith A. (2014). Stability Analysis of Steel Frame Structures: P-Delta Analysis. *IJRET: International Journal of Research in Engineering and Technology*, *03*(08), 2321–7308. http://www.ijret.org

Peker, K., Akgönen, A. İ., & Yardımcı, N. (2021). Investigation on seismic performance of weak-axis moment connections with European profiles. *Structures*, *32*, 254–267. https://doi.org/10.1016/j.istruc.2021.02.047

Petreski, B., & Gjorgjiev, I. (2021). Residual drift estimation for moment resisting frames with steel degradation properties. *Ce/Papers, 4*(2–4), 1917–1923. https://doi.org/10.1002/cepa.1504

Pour, M. (2022). Seismic damage assessment of steel buildings considering viscoelastic dampers in near-field earthquake. *Shock and Vibration, 2022*, 1–15. https://doi.org/10.1155/2022/2905960

Setiadi, A., Sarjana, T. A., Santoso, S. I., & Nurfadillah, S. (2021). Economic analysis comparison between broiler chicken reared in closed house cage and its reared in open house cage. *IOP Conference Series: Earth and Environmental Science*, *803*(1). https://doi.org/10.1088/1755-1315/803/1/012066

Shan, S., & Pan, W. (2020). Structural design of high-rise buildings using steel-framed modules: a case study in Hong Kong. *The Structural Design of Tall and Special Buildings, 29*(15). https://doi.org/10.1002/tal.1788

SNI-1726-2019-Persyaratan Beton Struktural Untuk Bangunan Gedung, Pub. L. No. SNI 1726:2019 (2019).

SNI-2847-2019 Persyaratan Beton Struktural Untuk Bangunan Gedung, Pub. L. No. SNI 2847:2019 (2019).

Tartaglia, R., Campiche, A., & Martino, A. (2021). Influence of the p-delta effect on the design of steel moment resisting frame in seismic areas. *Key Engineering Materials, 873*, 33–37.

The Structural Engineering Institute of ASCE. (2012). Advanced Analysis in Steel Frame Design. In *Advanced Analysis in Steel Frame Design*. American Society of Civil Engineers. https://doi.org/10.1061/9780784411964

Zavala, D., Torres, C., & Moreno, J. (2022). Influence of the p-delta effect and stiffness irregularity on the structural behavior of reinforced concrete buildings. *Journal of Physics: Conference Series, 2287*(1), 012047. https://doi.org/10.1088/1742-6596/2287/1/012047